

Geophysical Research Letters®



RESEARCH LETTER

10.1029/2023GL104134

Modeling Deep Rooted Thrust Mechanism of Crustal Thickening in Eastern Tibet

P. Pitard¹ , A. Replumaz¹ , C. Thieulot², and M.-P. Doin¹ 

¹University Grenoble Alpes, CNRS, USMB, IRD, IFSTTAR, ISTerre, Grenoble, France, ²Department of Earth Sciences, Utrecht University, Utrecht, the Netherlands

Key Points:

- 2-D numerical models of thrusts embedded in the high viscosity upper crust, to test thermo-kinematic models based on thermochronology data
- accommodation in the lower crust by ductile flow of the deformation induced by the high angle thrust in the upper crust
- predicting exhumation rates and subsidence patterns that are compatible with the measured ones in Eastern Tibet

Supporting Information:

Supporting Information may be found in the online version of this article.

Correspondence to:

A. Replumaz,
anne.replumaz@univ-grenobles-alpes.fr

Citation:

Pitard, P., Replumaz, A., Thieulot, C., & Doin, M.-P. (2023). Modeling deep rooted thrust mechanism of crustal thickening in Eastern Tibet. *Geophysical Research Letters*, 50, e2023GL104134. <https://doi.org/10.1029/2023GL104134>

Received 15 APR 2023

Accepted 15 JUL 2023

Author Contributions:

Conceptualization: A. Replumaz, C. Thieulot, M.-P. Doin
Formal analysis: P. Pitard
Funding acquisition: A. Replumaz
Investigation: A. Replumaz, C. Thieulot
Methodology: C. Thieulot
Project Administration: A. Replumaz
Software: C. Thieulot
Supervision: A. Replumaz, C. Thieulot, M.-P. Doin
Validation: A. Replumaz, C. Thieulot, M.-P. Doin
Visualization: P. Pitard, A. Replumaz

© 2023. The Authors.

This is an open access article under the terms of the [Creative Commons Attribution-NonCommercial-NoDerivs License](https://creativecommons.org/licenses/by-nc-nd/4.0/), which permits use and distribution in any medium, provided the original work is properly cited, the use is non-commercial and no modifications or adaptations are made.

Abstract To test Eastern Tibet crustal thickening modes, we compare 2-D numerical models of two emblematic end-member models, with either an obstacle in the low viscosity lower crust or a thrust embedded in the high viscosity one. We show that the obstacle halts the viscous lower crustal flow potentially initiated by the weight of the high Central Tibet, generating a smooth exhumation gradient at the edge of the plateau, not observed in Eastern Tibet. On the contrary, including a low viscosity discontinuity in the upper crust, mimicking a shallow steep listric fault as inferred in the region, reproduces a sharper exhumation profile, as constrained from thermo-kinematic inversions of thermochronological data, and the lack of foreland basin, as observed in the field. Moreover, such fault drives deformation throughout the entire crust, suggesting a deep crustal ductile shear zone limiting the more ductile deformation in the lower crust although no discontinuity is imposed.

Plain Language Summary The role of thrusting in crustal thickening during the formation of Tibet, the world's largest and highest orogenic plateau, constitutes one of the main controversies in earth sciences. In Eastern Tibet in particular, two end-members based on two contrasting controversial hypotheses can be tested: the thickening is dominated either by the flow of the lower Tibetan crust halted by the hard Sichuan craton, or by thrusting of the Tibetan upper crust. Here, we present 2-D crustal numerical models of a shallow steep listric thrust (as inferred in the region) embedded in the high viscosity upper crust, and we show that such model reproduces the exhumation profile constrained from thermochronological data and the lack of foreland basin observed in the field. Interestingly, we also show that such upper crustal thrust drives upward the more ductile lower crust albeit no discontinuity is imposed. On the contrary, by using a model driven by an overpressure in the lower crust, we show that the obstacle halts the viscous lower crustal flow and generates a smooth exhumation gradient at the edge of the plateau, not observed in Eastern Tibet.

1. Introduction

Despite decades of controversy, our understanding of the formation of the Tibetan Plateau remains limited. The role of competing mechanisms, such as distributed crustal thickening versus lateral propagation of thrust faulting at crustal or lithospheric scales, is still poorly understood. Conceptual models explaining observations at the continental scale are based on hypotheses that are hard to reconcile. On the one hand, buoyancy forces associated with very thick crust and a low-viscosity channel in the Tibetan crust may drive distributed outward flow of the partially molten middle crust toward the east caused by the weight of the high Central Tibet, with entrenchment of the rivers within relict peneplains contemporaneous of the uplift (“channel flow model,” Royden et al., 2008; Clark, Bush, & Royden, 2005). On the other hand, surface geological observations of fault systems favor the role of thrust faulting in the upper crustal thickening, while the lower crust subducts attached to the lithospheric mantle, with discrete outward propagation of thrusts since the onset of collision at ~50 Ma, through strike-slip faults, such as the XianShuiHe fault to the east (“stepwise model,” Tapponnier et al., 2001; Jiao et al., 2023). However, no numerical model considering the role of thrust faulting in the interaction between the lower and upper crusts has yet been implemented in Eastern Tibet in the stepwise model to be compared with the analytical dynamic pressure generated by the lower crustal flow used as the driving load for the flexure equation to compute a vertical deflection done for the channel flow model. Therefore, it remains difficult to test the mechanical and rheological consistency, and the ability to explain observations, of these end-member conceptual models.

In order to generate new insights in deformation modes in Tibet, we model the mechanical behavior of the crust under boundary conditions corresponding to both end-member models. We focus on the very contrasted Tibet

Writing – original draft: P. Pitard, A. Replumaz, C. Thieulot, M.-P. Doin

eastern edge, with to the northeast the Longmenshan thrust belt (LMTB) bounding the rigid Sichuan craton with a steep topographic gradient, and to the southeast the Yalong thrust belt (YTB) crossing the Yalong margin bounding the South China craton with a gentler topographic gradient. This key location has long been studied to propose different models of Tibetan Plateau formation (Figure 1). In this region, a collection of multi-scale data is available that we use to constrain the models, including a dense thermochronologic data set thanks to numerous granite outcrops in Eastern Tibet compared to mostly sedimentary rocks in Central Tibet (e.g., Clark, House, et al., 2005; Pitard et al., 2021). At depth, receiver function profiles (Robert et al., 2010) and regional shear waves tomography images (Yao et al., 2008) show a sharp ~20 km step of the Moho depth between the plateau (~60–63 km) and the Sichuan craton (~40 km) across the LMTB, and a ~15 km smoother transition in crustal thickness across the YTB between the plateau (~60–63 km) and the South China craton (45–50 km) (Figure 1). In the channel flow model, mid-crustal flow is halted in the Longmenshan by the rigid Sichuan craton, inducing topographic growth at its border as in the high-standing LMTB (Figure 1c). Across the Yunnan margin, flow is continuous in the absence of obstacle in the lower crust, generating a smooth topographic gradient with no spatial discontinuity and no thickening of the upper crust (Clark, Bush, & Royden, 2005). By contrast, in the stepwise model of Tapponnier et al. (2001), discrete thrust faults of the YTB merge on an intracrustal decollement, allowing the thickening of the upper crust and forming topographic steps (Figure 1b).

In this paper, we present 2-D numerical models of thrust embedded in the high viscosity upper crust (model 1 under “lateral constant velocity” representing the eastward motion of Tibet shown by the GPS velocity field, reproducing the “stepwise model” boundary conditions), in which upper crustal thrust geometry is based upon thermo-kinematic modeling of thermochronology data. We compare with models with no fault but showcasing an obstacle in the lower crust (model 2 under “Poiseuille velocity” representing the velocity field generating by the weight of the high Central Tibet in a lower crustal channel, reproducing the “channel flow model” boundary conditions), which setup is based upon analytical dynamic pressure result. We test the short-term mechanical consistency of the fault geometry for varying fault and lower crust viscosity to shed light on end-member mechanisms of Tibetan plateau formation. Such modeling allows to include the localisation of deformation on faults in the long-term history of building the Tibetan Plateau, to quantify the mechanisms of crustal thickening up to the modern value of ~65 km (Figure 1).

2. Geological and Geophysical Constraints on the Crustal Structure of Tibet Eastern Edge

The LMTB at the western margin of the Sichuan basin (Figure 1) is active, as attested by major earthquakes, such as the 2008 Mw7.9 Wenchuan earthquake. During the earthquake, thrusts ruptured with steep shallow ramps (up to 70°), rooting between 15 and 25 km-depth on a sub-horizontal décollement zone at the brittle-ductile transition (e.g., de Michele et al., 2010; Fielding et al., 2013; Hubbard & Shaw, 2009). On the longer term, high exhumation rate above the ramp and low above the décollement have been measured using thermochronology (e.g., Li et al., 2023). It has been proposed that brittle deformation occurs in the thick upper crust above the décollement, a Cretaceous passive margin with a thick sedimentary wedge, while the thin lower crust remain mostly passive (e.g., Airaghi et al., 2018). It has also been proposed that the brittle deformation observed in the upper crust has been induced by the lower crust flow, above the location where the flow is deviated upward, with no foreland flexural basin in the footwall (e.g., Burchfiel et al., 2008). Last, considering that the LMTB coincides with the limit of a low shear velocity layer in the middle and lower crusts which limits the southeastward extent of the thickened Tibetan crust, it has been proposed that thrusts should extend in the lower crust (Robert et al., 2010) (Figure 1c).

Across the Yalong margin, the YTB is present-day inactive, with no reverse focal mechanism observed. On the longer term, the Muli thrust of the YTB shows a thermochronology age zonation parallel to the fault, with Miocene ages (<10 Ma) close to the thrust, rapidly becoming older away from it (Clark, House, et al., 2005; Pitard et al., 2021). Such spatial distribution of the ages is best reproduced by a listric thrust geometry, at a velocity rate of 0.26 km/Ma until 11.5 Ma then at a faster rate of 0.52 km/Ma, yielding since 50 Ma to a total of ~15 km of exhumation along the uppermost crustal high-angle ramp and ~8 km above the sub-horizontal deep décollement (Pitard et al., 2021) (Figure 1e). The depth of the intra-crustal décollement is not well constrained at depth greater than 20 km, as the thermochronometers are only sensible to upper crustal thermal evolution. On the contrary, the age zonation could not be reproduced only by the entrenchment of the Yalong River as proposed in the channel flow model (Clark, House, et al., 2005), with too old ZHe and AFT ages predicted (Figure 1e).

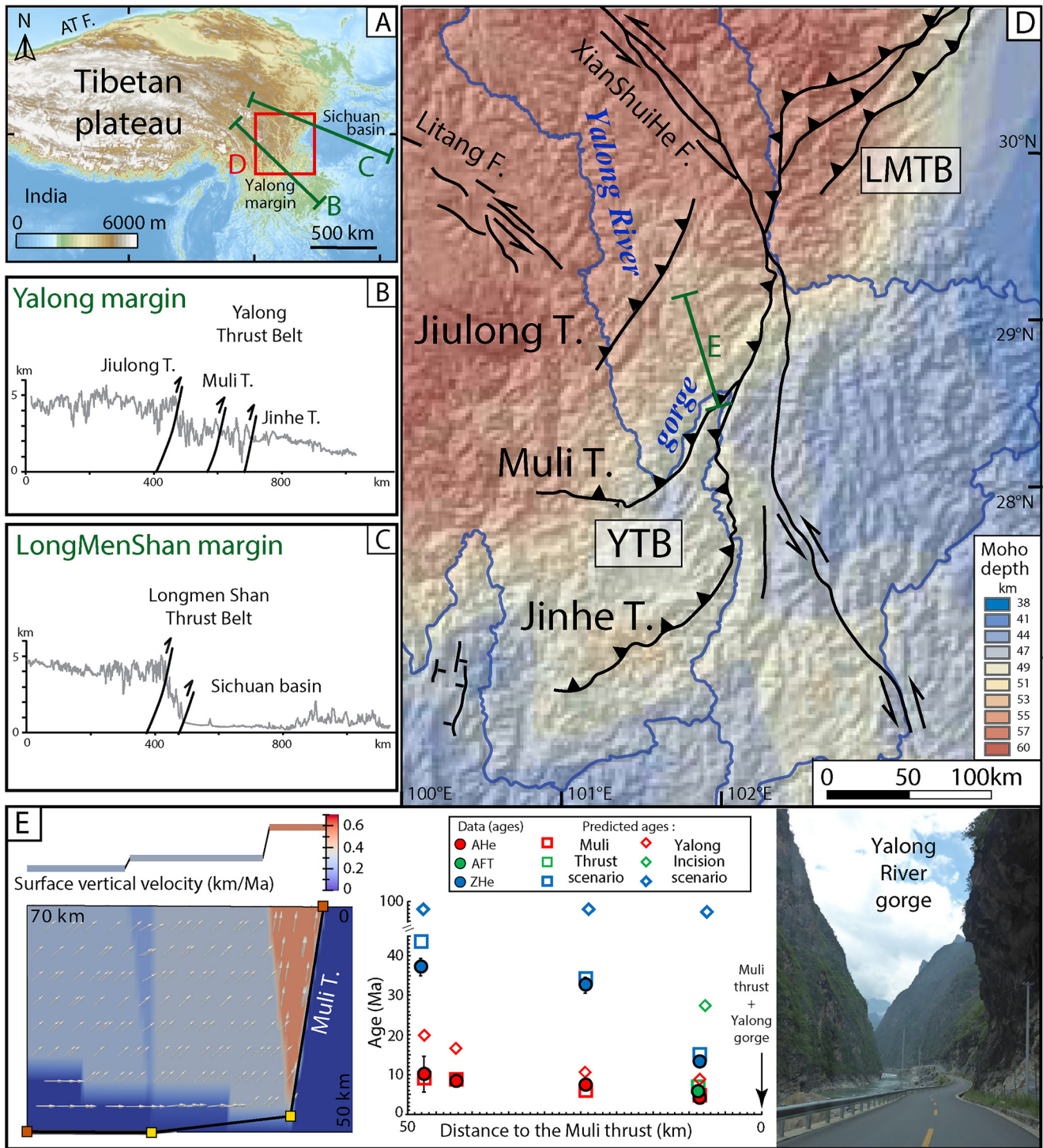


Figure 1. A/Location of the Yalong margin, South-East Tibet. AT F.: Altyn Tagh fault. B/and C/Topographic profiles across the Yalong and the LongMenShan margins (see A/for location). D/Moho depth map (Yao et al., 2008), with main faults, LMTB: Longmenshan thrust belt, YTB: Yalong thrust belt including the Jiulong, Muli and Jinhe thrusts (T.), XianShuiHe and Litang strike-slip faults (F.). E/2-D crustal velocity field obtained by inversion of thermochronology ages with corresponding measured and predicted ages (AHe and ZHe: Apatite or Zircon (U-Th)/He, AFT: Apatite fission track) for the tectonics scenario of exhumation above the Muli thrust (square) (Pitard et al., 2021), to be compared with an incision scenario (diamond) of exhumation due to the incision of the Yalong River, illustrated by a picture of the deep gorge where the river crosses the thrust.

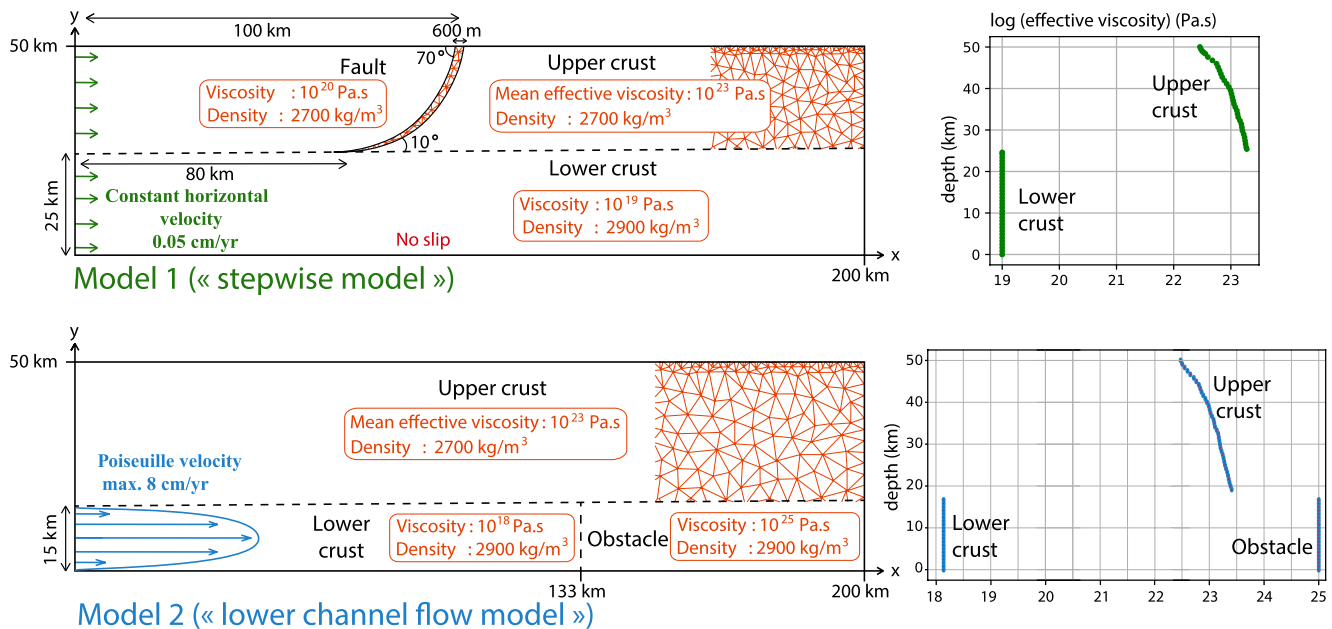


Figure 2. 2D crustal mechanical models setup with effective viscosity of a pseudo-plastic behavior for the upper crust (mean value 10^{23} Pa.s), constant viscosity for the lower crust (10^{19} Pa.s in model 1, 10^{18} Pa.s in model 2), the fault in model 1 (10^{20} Pa.s) and the obstacle in model 2 (10^{25} Pa.s). Deformation under a constant horizontal velocity in model 1, or under a Poiseuille flow in model 2, no-slip basal condition.

3. Method: 2-D Mechanical Models of a Viscous Crust

A 2-D code has been developed in which the Stokes equations are solved for an incompressible Newtonian fluid on a Lagrangian grid (Pitard et al., 2023). We define a rectangular box of $200 \text{ km} \times 50 \text{ km}$ with four different zones for which we can assign different values of viscosities and densities (Figure 2). Two horizontal layers correspond to the upper and lower crust. Viscosity is constant within the lower crust in model 1, while in model 2, the lower crust is separated in two blocks, with the high viscosity one on the right mimicking a rigid obstacle. Viscosity within the upper crust is computed with a plastic yield stress increasing with depth to simulate a more realistic crustal rheological profile corresponding to a traditional model of a Quartzo-feldspathic crust (Burov & Watts, 2006; Chen & Molnar, 1983). It defines a high strength upper crust and a ductile lower crust with analogy to the jam layer of a jelly sandwich (Bürgmann & Dresen, 2008). In model 1, a fault is mimicked in the upper crust by a thinly meshed constant-width zone of lower viscosity (Figure 2). Such low viscosity in the fault, three order of magnitude lower than for the upper crust, simulates a weak fault with low shear stresses, often reproduced in model by strain-softening (e.g., Buitert et al., 2006; Huisman & Beaumont, 2003).

The triangle mesh is deforming at each time step. The time stepping is adaptive, following the CFL condition (van Zelst et al., 2022). The boundary conditions of the model are as follows: convergence is imposed on the left side of the box, with a constant horizontal velocity (model 1, “stepwise model” boundary conditions) or a Poiseuille horizontal velocity in the lower crust and zero velocity in the upper crust (model 2, “lower channel flow model” boundary conditions). The right side is a closed boundary. Vertical velocity is allowed on both sides with a zero shear stress boundary condition. The top boundary of the box is a free surface, allowing the growth of topography, while the bottom boundary condition is no slip with no vertical velocity.

4. Results for Endmember Models: “Lateral Constant Velocity” Versus “Poiseuille Velocity”

In the model 1 (stepwise model), to mechanically test the accommodation at depth by ductile flow of the shallow kinematic velocity field induced by the high angle of the Muli thrust, constant horizontal velocity condition of 0.05 cm/yr are imposed on the western side of the model, representing the eastward motion of Tibet shown by the GPS velocity field (e.g., Wang et al., 2001). To mimic a shallow high angle listric fault (70° dip), a discontinuity with a lower viscosity of 10^{20} Pa.s is introduced in the upper crust with a listric shape and a steep shallow

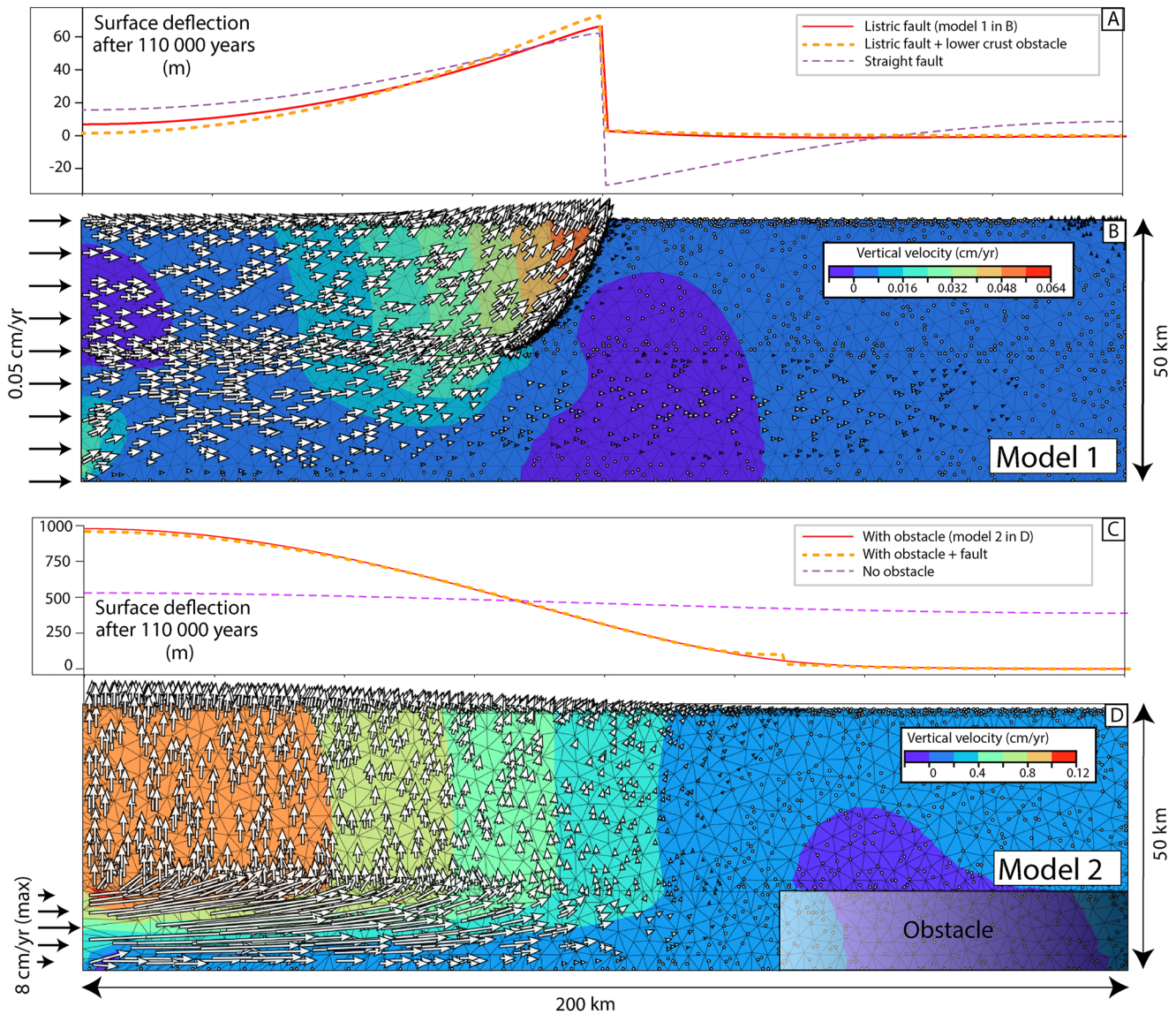


Figure 3. A/Surface deflection and B/velocity field of model 1, deforming under constant horizontal velocity boundary condition, and a fault embedded in the upper crust. C/Surface deflection and D/Velocity field of model 2, deforming under Poiseuille flow condition in the lower crust.

dip. Under this constant lateral kinematical boundary condition, the upper crust moves horizontally close to the moving boundary, and progressively moves upward toward the fault, reaching a maximum vertical velocity of ~ 0.06 cm/yr, that is, ~ 0.6 km/Ma (Figure 3b). It corresponds to an increase of the uplift of the surface toward the fault, less than 10 m 100 km away from the fault and more than 60 m near the fault after 110,000 years (Figure 3a). Interestingly, the lower crust moves horizontally close to the moving boundary, but also progressively moves upward toward the fault, even if the fault does not extend at depth. The velocity magnitude is higher in the lower crust than in the upper one until the flow reaches the position of the fault, with a rapid decrease of the horizontal velocity. A complete parametric study has been carried out (see Supporting Information S1), to systematically test the influence of each parameter (viscosities within the fault and the lower crust, lower crustal thickness, fault width and geometry, lateral velocity, background strain rate, cohesive strength, friction angle in the upper crust), before choosing the parameter values of model 1, so that the velocity gradient toward the fault is similar to the exhumation gradient obtained by thermo-kinematic modeling based on thermochronology data (Figure 1e). By changing the geometry of the fault, we show that with a straight fault the surface velocity is much more symmetric, showing a strong subsidence in the footwall (Figure 3a, Figure S5 in Supporting Information S1). It is worth

noting that adding a rigid lower crust obstacle with a listric upper crustal fault does not change the velocity profile (Figure S9 in Supporting Information S1).

The fault is absent in model 2 (lower channel flow model) but a rigid block is present in the lower crust, acting as a barrier to the flow, with a Poiseuille velocity boundary condition in the lower crust (Figure 3d). The maximum horizontal velocity imposed on the left boundary is 8 cm/yr (Clark & Royden, 2000), the optimum published value to reproduce the topography of the LMTB (Figure 1c). It has been obtained with analytical model of dynamic overpressure within a lower crustal channel of 15 km width. Under these Poiseuille velocity boundary conditions, but considering the upper and lower crust as incompressible Newtonian fluid with different values of viscosities and densities (Figure 2), the horizontal lower crustal motion is transmitted to vertical motion in the upper crust (Figure 3d). The maximum vertical velocity is of 0.94 cm/yr on the left boundary of the box, leading after ~100,000 years to ~1 km of positive deflection, decreasing to ~300 m above the obstacle edge, and no deflection above the rigid obstacle (Figure 3d). A complete parametric study has also been carried out (see Supporting Information S1). In particular, we show that without the obstacle in the lower crust, the velocity profile is much smoother, almost horizontal (Figure 3c). Interestingly, with a fault in the upper crust, only a small local perturbation is observed above the fault (Figure 3c), corresponding to a minor flow in the upper crust driven by the fault (S15).

5. Discussion: Comparison of Model Predictions With Morphotectonic Observations

We compare the modeled deflection profiles with the exhumation profile constrained by thermochronologic ages for the Muli thrust of the YTP crossing the Yalong margin (Figure 1e). Such exhumation profile is more pertinent for a quantitative comparison with the modeled deflection profile, as erosion that shaped the topography during and after the tectonic uplift is not included in our models. Previously, only the topographic profiles have been used, showing smoother topographic steps across the YTB than across the LMTB (Figure 1).

5.1. Lower Crust Channel Flow Model

In the channel flow model, no obstacle has been inferred for the Yalong margin and a smooth topographic step has been calculated (Clark, Bush, & Royden, 2005). Our numerical results showcase a very different deflection profile which is almost flat (Figure 3c). Such profile is not comparable with the sharp exhumation profile of the Muli thrust, with a sharp positive deflection above the thrust (Figure 1). Furthermore, in the Yalong margin region, the channel flow scenario has been related to a regional uplift of low-relief surfaces where exhumation is mainly driven by deeply entrenched river incision. By testing such scenario on the complete thermochronologic data set available for the Muli thrust (Pitard et al., 2021), we show that incision alone is not reproducing the thermochronologic ages (Figure 1e).

Nevertheless, assuming that the South China craton is comparable with the Sichuan craton, as seen in tomography models (Yao et al., 2008), with a positive velocity anomaly in the foreland of the Yalong margin (Figure 4), we also compare the Yalong margin with the model including an obstacle in the lower crust. In the channel flow model, such obstacle is mimicking the Sichuan craton stopping the eastward weak lower crust flow below the LongmenShan range (Clark & Royden, 2000), the dynamic pressure at the edge of the obstacle generating an overpressure localizing the thrusts in the upper crust (Burchfiel et al., 2008). Using the published strikingly high velocity calculated for the flow to fit the topographic step observed in the LongmenShan range above the LMTB (8 cm/yr), a value that is unrealistic in nature, a symmetric negative vertical flexural deflection has been obtained on the other side of the obstacle (Clark & Royden, 2000). First, such negative deflection in the footwall of the LMTB is not observed in the field, and such a lack of foreland flexural basin has been pointed out as a peculiar characteristic for such high mountain range (Burchfiel et al., 2008), so that regional topography deduced from flexure equation (Clark & Royden, 2000) is not pertinent. Second, by testing such boundary conditions in our model 2, we show that the rapid flow in the lower crust leads to the thickening of the crust with unrealistic rapid growth of the topography (1 km in 110,000 years, Figure 3d), but also with a very different deflection profile, smooth with a gradual decrease of the velocity being almost null at the edge of the obstacle (Figure 3c). Such smooth deflection profile is not comparable with the sharp exhumation profile of the YTB (Figure 1e) at the edge of the South China craton (Figure 4), similar to the one of the LMTB at the edge of the Sichuan craton (e.g., Li et al., 2023). Indeed, by adding a thrust in the upper crust at the edge of the obstacle (Figure S15 in Supporting

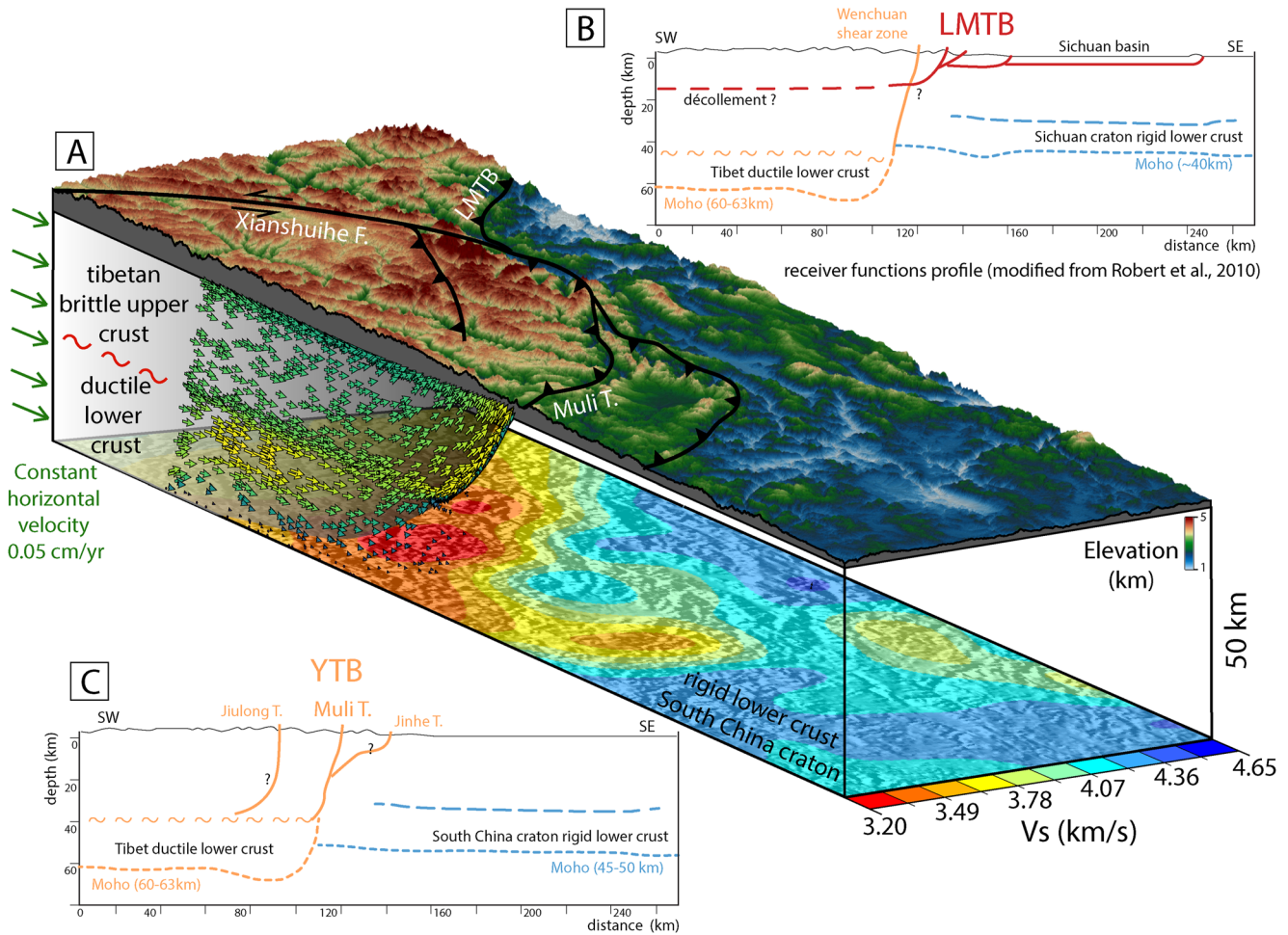


Figure 4. A/3D block diagram of the Yalong margin with surface topography (2X vertical exaggeration, Pitard et al., 2021), tomography section at 50 km-depth (Yao et al., 2008), and the 2D crustal velocity field of our model 1, with constant lateral push, where shallow the high angle listric Muli thrust acts as a ramp to exhume crustal material. B/2D vertical section across the LongMenShan Thrust Belt (LMTB) drawn from the receiver function profile of Robert et al. (2010). C/2D vertical section across the Yalong margin, modified from B, showing a similar crustal geometry inferred for the Yalong Thrust Belt (YTB).

Information S1), as the lower crust flow is not reaching the edge of the obstacle, such thrust is not playing a significant role in limiting the deformation, unlike what it is observed in SE Tibet (Figure 1).

5.2. Low Viscosity Thrust Embedded in the Upper Crust

With a straight fault geometry, the deflection profile is symmetric, with a negative deflection in the footwall of the thrust (Figure 3a), which does not agree with the lack of foreland flexural basin observed in the footwall of both the YTB and LMTB (Burchfiel et al., 2008). On the contrary, the deflection profile obtained in our model 1 with a listric fault (Figure 3b), is comparable to the exhumation profile measured for the Yalong margin, with a sharp positive deflection above the Muli thrust and no symmetric negative deflection above the foreland (Figure 1c). For the hanging wall, the thermo-kinematic inversion of the thermochronological data obtains an exhumation rate between 0.26 and 0.52 km/Ma (Pitard et al., 2021), of the same order of magnitude than the rate at 0.6 km/Ma obtained in our model (Figure 3a). The maximum total exhumation is of ~15 km close to the Muli fault trace (Figure 1e), corresponding in nature, where erosion at the edge of the plateau is active, to a smooth topographic step of ~2 km (Figure 1b). Such quantitative and qualitative difference makes the comparison of the model deflection with only the topographic profile not pertinent.

However, the velocity field near the Muli thrust is constrained only in the first 20 km of the crust by thermochronological data (Pitard et al., 2021). Our 2-D numerical modeling overcome such limitations raised

by thermo-kinematic modeling, in particular for the implied viscous flow in the lower crust. Indeed, our model 1 shows that the listric thrust in the upper crust influences deformation throughout the entire crust, limiting the propagation of the flow in the lower crust below the fault, albeit no discontinuity is imposed (Figure 3b). The regional tomographic images show that the crustal thickening stops at the Muli thrust (Yao et al., 2008). It suggests that the limit of the more ductile deformation in the lower crust is driven by the upper crustal Muli thrust, extending at depth by a ductile shear zone that could reach the base of the crust (Robert et al., 2010), acting as a ramp to exhume crustal material to the surface (Figure 4). On the contrary, in North Tibet, the lower crust appears rigid and subducts attached to the lithospheric mantle, while thrusts are branching at depth on an intracrustal decollement, thickening only the upper crust (e.g., Lin et al., 2022; Meyer et al., 1998).

Adding a rigid obstacle in the lower crust mimicking the South China craton is not modifying the deflection profile (Figure 3a), but in our setup we impose the position of the upper crust thrust (Figure 2), while in nature the thrust belts are located at the edge of the cratons (Figure 4). Indeed, the LMTB is located at the edge of the Sichuan craton, extending at depth and marking a strong crustal contrast (Robert et al., 2010) (Figure 1c). The YTB is also at the edge of the South China craton, and we conclude to a structure at depth similar to the one of the LMTB, with the Muli thrust being the dominant structure (Figure 4). Nevertheless, with respect to the LMTB, the YTB is spreading more over the craton, making a smoother topographic transition between the high plateau and the foreland (Figure 1b). Such spreading is most probably due to the propagation of crustal thickening along the strike-slip fault of XianShuiHe, as shown in the north of the plateau along the Altyn Tagh fault (Jiao et al., 2023; Tapponnier et al., 2001).

6. Conclusion: Implication for Crustal Thickening Processes of Eastern Tibet

We conclude that structural, topographic, tomography, thermochronology, and thermo-kinematic modeling data from the Yalong thrust belt region contradict the hypothesis of a fast flow in a lower crust channel, but favor the model where shallow high angle listric thrusts (70° dip) act as a ramp to exhume crustal material to the surface. Our modeling yields the thickening of the entire crust, with a thick, warmer and therefore more ductile lower crust (Figure 4) as seen on tomographic images. In this region (LongmenShan and Yalong margins), the former passive margin structure of the SongPan Ganze block with a thick sedimentary wedge and a thinned lower crust (e.g., Airaghi et al., 2018; Roger et al., 2010), bounding the rigid Sichuan and South China craton (Yao et al., 2008), probably leads to this peculiar deformation regime.

Data Availability Statement

The code used for this paper can be found at <https://doi.org/10.5281/zenodo.7558920> (Pitard et al., 2023).

References

- Airaghi, L., De Sigoyer, J., Guillot, S., Robert, A., Warren, C., & Deldicque, D. (2018). The Mesozoic along-strike tectonometamorphic segmentation of Longmen Shan (eastern Tibetan plateau). *Tectonics*, 37(12), 4655–4678. <https://doi.org/10.1029/2018TC005005>
- Buiter, S. J. H., Babeyko, A. Y., Ellis, S., Gerya, T. V., Kaus, B. J. P., Kellner, A., et al. (2006). The numerical sandbox: Comparison of model results for a shortening and an extension experiment, Book Series. *Geological Society - Special Publications*, 253(1), 29–64. <https://doi.org/10.1144/GSL.SP.2006.253.01.02>
- Burchfiel, B. C., Royden, L. H., Van der Hilst, R. D., Hager, B. H., Chen, Z., King, R., et al. (2008). A geological and geophysical context for the Wenchuan earthquake of 12 May 2008, Sichuan, People's Republic of China. *Geological Society of America Today*, 18(7), 4–11. <https://doi.org/10.1130/GSATG18A.1>
- Bürgmann, R., & Dresen, G. (2008). Rheology of the lower crust and upper mantle: Evidence from rock mechanics, geodesy, and field observations. *Annual Review of Earth and Planetary Sciences*, 36(1), 531–567. <https://doi.org/10.1146/annurev.earth.36.031207.124326>
- Burov, E., & Watts, A. (2006). The long-term strength of continental lithosphere: "jelly sandwich" or "crème brûlée"? *Geological Society of America Today*, 16(1), 4–10. [https://doi.org/10.1130/1052-5173\(2006\)016<4:tlSOc>2.0.CO;2](https://doi.org/10.1130/1052-5173(2006)016<4:tlSOc>2.0.CO;2)
- Chen, W.-P., & Molnar, P. (1983). Focal depths of intracontinental and intraplate earthquakes and their implications for the thermal and mechanical properties of the lithosphere. *Journal of Geophysical Research*, 88(B5), 4183–4214. <https://doi.org/10.1029/jb088ib05p04183>
- Clark, M. K., Bush, J. W., & Royden, L. H. (2005). Dynamic topography produced by lower crustal flow against rheological strength heterogeneities bordering the Tibetan plateau. *Geophysical Journal International*, 162(2), 575–590. <https://doi.org/10.1111/j.1365-246X.2005.02580.x>
- Clark, M. K., House, M. A., Royden, L. H., Whipple, K. X., Burchfiel, B. C., Zhang, X., & Tang, W. (2005). Late Cenozoic uplift of southeastern Tibet. *Geology*, 33(6), 525–528. <https://doi.org/10.1130/G21265.1>
- Clark, M. K., & Royden, L. H. (2000). Topographic ooze: Building the eastern margin of Tibet by lower crustal flow. *Geology*, 28(8), 703–706. [https://doi.org/10.1130/0091-7613\(2000\)28%3C703:TOBTEM%3E2.0.CO;2](https://doi.org/10.1130/0091-7613(2000)28%3C703:TOBTEM%3E2.0.CO;2)

Acknowledgments

This work was supported by the Agence Nationale de Recherche (ANR-20-CE49-PCR "Tibetan Orchestra").

- de Michele, M., Raucoules, D., de Sigoyer, J., Pubellier, M., & Chamot-Rooke, N. (2010). Three-dimensional surface displacement of the 2008 May 12 Sichuan earthquake (China) derived from Synthetic Aperture Radar: Evidence for rupture on a blind thrust. *Geophysical Journal International*, *183*(3), 1097–1103. <https://doi.org/10.1111/j.1365-246X.2010.04807.x>
- Fielding, E. J., Sladen, A., Li, Z., Avouac, J.-P., Bürgmann, R., & Ryder, I. (2013). Kinematic fault slip evolution source models of the 2008 M7.9 Wenchuan earthquake in China from SAR interferometry, GPS and teleseismic analysis and implications for Longmen Shan tectonics. *Geophysical Journal International*, *194*(2), 1138–1166. <https://doi.org/10.1093/gji/ggt155>
- Hubbard, J., & Shaw, J. H. (2009). Uplift of the Longmen Shan and Tibetan plateau, and the 2008 wenchuan (m= 7.9) earthquake. *Nature*, *458*(7235), 194–197. <https://doi.org/10.1038/nature07837>
- Huismans, R. S., & Beaumont, C. (2003). Symmetric and asymmetric lithospheric extension: Relative effects of frictional-plastic and viscous strain softening. *Journal of Geophysical Research*, *108*(B10), 2496. <https://doi.org/10.1029/2002JB002026>
- Jiao, L., Tapponnier, P., Donzé, F.-V., Scholtès, L., Gaudemer, Y., & Xu, X. (2023). Discrete element modeling of southeast Asia's 3D lithospheric deformation during the Indian collision. *Journal of Geophysical Research: Solid Earth*, *128*(1), e2022JB025578. <https://doi.org/10.1029/2022JB025578>
- Li, Z., Kamp, P. J., Liu, S., Xu, G., Tong, K., Danišik, M., et al. (2023). Late Cretaceous–Cenozoic thermal structure and exhumation of the Eastern Tibetan Plateau margin and its orogenic wedge. *Earth-Science Reviews*, *238*, 104319. <https://doi.org/10.1016/j.earscirev.2023.104319>
- Lin, X., Jolivet, M., Liu-Zeng, J., Cheng, F., Wu, Z., Tian, Y., et al. (2022). The formation of the North Qilian Shan through Time: Clues from detrital zircon fission-track data from modern river sediments. *Geosciences*, *12*(4), 166. <https://doi.org/10.3390/geosciences12040166>
- Meyer, B., Tapponnier, P., Bourjot, L., Metivier, F., Gaudemer, Y., Peltzer, G., et al. (1998). Crustal thickening in gansu-qinghai, lithospheric mantle subduction, and oblique, strike-slip controlled growth of the tibet plateau. *Geophysical Journal International*, *135*, 1–47. <https://doi.org/10.1046/j.1365-246x.1998.00567.x>
- Pitard, P., Replumaz, A., Chevalier, M.-L., Leloup, P.-H., Bai, M., Doin, M.-P., et al. (2021). Exhumation history along the muli thrust—Implication for crustal thickening mechanism in eastern Tibet. *Geophysical Research Letters*, *48*(14), e2021GL093677. <https://doi.org/10.1029/2021GL093677>
- Pitard, P., Replumaz, A., Thieulot, C., & Doin, M.-P. (2023). Modelling deep rooting thrust mechanism of crustal thickening in Eastern Tibet. *Zenodo*. <https://doi.org/10.5281/zenodo.7558920>
- Robert, A., Pubellier, M., de Sigoyer, J., Vergne, J., Lahfid, A., Cattin, R., et al. (2010). Structural and thermal characters of the Longmen Shan (Sichuan, China). *Tectonophysics*, *491*(1–4), 165–173. <https://doi.org/10.1016/j.tecto.2010.03.018>
- Roger, F., Jolivet, M., & Malavieille, J. (2010). The tectonic evolution of the Songpan-Garzê (North Tibet) and adjacent areas from Proterozoic to present: A synthesis. *Journal of Asian Earth Sciences*, *39*(4), 254–269. <https://doi.org/10.1016/j.jseas.2010.03.008>
- Royden, L. H., Burchfiel, B. C., & van der Hilst, R. D. (2008). The geological evolution of the Tibetan plateau. *Science*, *321*(5892), 1054–1058. <https://doi.org/10.1126/science.1155371>
- Tapponnier, P., Zhiqin, X., Roger, F., Meyer, B., Arnaud, N., Wittlinger, G., & Jingsui, Y. (2001). Oblique stepwise rise and growth of the Tibet plateau. *Science*, *294*(5547), 1671–1677. <https://doi.org/10.1126/science.105978>
- van Zelst, I., Crameri, F., Pusok, A. E., Glerum, A., Dannberg, J., & Thieulot, C. (2022). 101 geodynamic modelling: How to design, interpret, and communicate numerical studies of the solid Earth. *Solid Earth*, *13*(3), 583–637. <https://doi.org/10.5194/se-13-583-2022>
- Wang, Q., Zhang, P. Z., Freymueller, J. T., Bilham, R., Larson, K. M., Lai, X., et al. (2001). Present-day crustal deformation in China constrained by global positioning system measurements. *Science*, *294*(5542), 574–577. <https://doi.org/10.1126/science.1063647>
- Yao, H., Beghein, C., & van der Hilst, R. D. (2008). Surface wave array tomography in SE Tibet from ambient seismic noise and two-station analysis. *Geophysical Journal International*, *173*(1), 205–219. <https://doi.org/10.1111/j.1365-246X.2007.03696.x>

References From the Supporting Information

- Alejano, L. R., González, J., & Muralha, J. (2012). Comparison of different techniques of tilt testing and basic friction angle variability assessment. *Rock Mechanics and Rock Engineering*, *45*(6), 1023–1035. <https://doi.org/10.1007/s00603-012-0265-7>
- Beaumont, C., Jamieson, R. A., Nguyen, M. H., & Lee, B. (2001). Himalayan tectonics explained by extrusion of a low-viscosity crustal channel coupled to focused surface denudation. *Nature*, *414*(6865), 738–742. <https://doi.org/10.1038/414738a>
- Byerlee, J. (1978). Friction of rocks. In *Rock friction and earthquake prediction* (pp. 615–626).
- Coulson, J. H. (1972). Shear strength of flat surfaces in rock. In *Stability of rock slopes* (pp. 77–105).
- Doin, M. P., Twardzik, C., Ducret, G., Lasserre, C., Guillaso, S., & Jianbao, S. (2015). InSAR measurement of the deformation around Siling Co Lake: Inferences on the lower crust viscosity in central Tibet. *Journal of Geophysical Research: Solid Earth*, *120*(7), 5290–5310. <https://doi.org/10.1002/2014jb011768>
- England, P. C., Walker, R. T., Fu, B., & Floyd, M. A. (2013). A bound on the viscosity of the Tibetan crust from the horizontality of palaeolake shorelines. *Earth and Planetary Science Letters*, *375*, 44–56. <https://doi.org/10.1016/j.epsl.2013.05.001>
- Henriquet, M., Avouac, J. P., & Bills, B. G. (2019). Crustal rheology of southern Tibet constrained from lake-induced viscoelastic deformation. *Earth and Planetary Science Letters*, *506*, 308–322. <https://doi.org/10.1016/j.epsl.2018.11.014>
- Hilley, G. E., Bürgmann, R., Zhang, P. Z., & Molnar, P. (2005). Bayesian inference of plastosphere viscosities near the Kunlun Fault, northern Tibet. *Geophysical Research Letters*, *32*(1), L01302. <https://doi.org/10.1029/2004gl021658>
- Ryder, I., Bürgmann, R., & Pollitz, F. (2011). Lower crustal relaxation beneath the Tibetan plateau and Qaidam basin following the 2001 Kokoxili earthquake. *Geophysical Journal International*, *187*(2), 613–630. <https://doi.org/10.1111/j.1365-246x.2011.05179.x>
- Shewchuk, J. R. (1996). Triangle: Engineering a 2D quality mesh generator and Delaunay triangulator. In *Workshop on applied computational geometry* (pp. 203–222). Springer Berlin Heidelberg.
- Shewchuk, J. R. (2002). Delaunay refinement algorithms for triangular mesh generation. *Computational Geometry*, *22*(1–3), 21–74. [https://doi.org/10.1016/s0925-7721\(01\)00047-5](https://doi.org/10.1016/s0925-7721(01)00047-5)
- Taylor, S. R., & McLennan, S. M. (1985). The continental crust: Its composition and evolution.
- Turcotte, D. L., & Schubert, G. (2002). *Geodynamics*. Cambridge university press.
- Wen, Y., Li, Z., Xu, C., Ryder, I., & Bürgmann, R. (2012). Postseismic motion after the 2001 Mw 7.8 Kokoxili earthquake in Tibet observed by InSAR time series. *Journal of Geophysical Research*, *117*(B8), B08405. <https://doi.org/10.1029/2011jb009043>
- Yamasaki, T., & Houseman, G. A. (2012). The crustal viscosity gradient measured from post-seismic deformation: A case study of the 1997 Manyi (Tibet) earthquake. *Earth and Planetary Science Letters*, *351*, 105–114. <https://doi.org/10.1016/j.epsl.2012.07.030>